A&A 499, 653–660 (2009)
DOI: 10.1051/0004-6361/200911847

Astronomy & Astrophysics

The core-collapse rate from the Supernova Legacy Survey

G. Bazin[1], N. Palanque-Delabrouille[1], J. Rich[1], V. Ruhlmann-Kleider[1], E. Aubourg[1,2], L. Le Guillou[3], P. Astier[3], C. Balland[3,4], S. Basa[5], R. G. Carlberg[7], A. Conley[7], D. Fouchez[8], J. Guy[3], D. Hardin[3], I. M. Hook[10], D. A. Howell[7], R. Pain[3], K. Perrett[7], C. J. Pritchet[9], N. Regnault[3], M. Sullivan[10], P. Antilogus[3], V. Arsenijevic[11], S. Baumont[3], S. Fabbro[11], J. Le Du[8], C. Lidman[12], M. Mouchet[2,6], A. Mourão[11], and E. S. Walker[10]

[1] CEA/Saclay, DSM/Irfu/Spp, 91191 Gif-sur-Yvette Cedex, France
e-mail: rich@hep.saclay.cea.fr
[2] APC, UMR 7164 CNRS, 10 rue Alice Domon et Léonie Duquet, 75205 Paris Cedex 13, France
[3] LPNHE, CNRS-IN2P3 and Universities of Paris 6 & 7, 75252 Paris Cedex 05, France
[4] University Paris 11, 91405 Orsay, France
[5] LAM, CNRS, BP8, Pôle de l'étoile, Site de Château-Gombert, 38 rue Frédéric Joliot-Curie, 13388 Marseille Cedex 13, France
[6] LUTH, UMR 8102 CNRS, Observatoire de Paris, Section de Meudon, 92195 Meudon Cedex, France
[7] Deparment of Astronomy and Astrophysics, University of Toronto, 50 St. George Street, Toronto, ON M5S 3H8, Canada
[8] CPPM, CNRS-Luminy, Case 907, 13288 Marseille Cedex 9, France
[9] Department of Physics and Astronomy, University of Victoria, PO Box 3055, Victoria, BC V8W 3P6, Canada
[10] University of Oxford, Astrophysics, Denys Wilkinson Building, Kneble Road, Oxford OX1 3RH, UK
[11] CENTRA-Centro M. de Astrofisica and Department of Physics, IST, Lisbon, Portugal
[12] European Southern Observatory, Alonso de Cordova 3107, Vitacura, Casilla 19001, Santiago 19, Chile

Received 13 February 2009 / Accepted 6 April 2009

ABSTRACT

We use three years of data from the Supernova Legacy Survey (SNLS) to study the general properties of core-collapse and type Ia supernovae. This is the first such study using the "rolling search" technique which guarantees well-sampled SNLS light curves and good efficiency for supernovae brighter than $i' \sim 24$. Using host photometric redshifts, we measure the supernova absolute magnitude distribution down to luminosities 4.5 mag fainter than normal SNIa. Using spectroscopy and light-curve fitting to discriminate against SNIa, we find a sample of 117 core-collapse supernova candidates with redshifts $z < 0.4$ (median redshift of 0.29) and measure their rate to be larger than the type Ia supernova rate by a factor $4.5 \pm 0.8(stat.) \pm 0.6(sys.)$. This corresponds to a core-collapse rate at $z = 0.3$ of $[1.42 \pm 0.3(stat.) \pm 0.3(sys.)] \times 10^{-4}$ yr$^{-1}(h_{70}^{-1}$ Mpc$)^{-3}$.

Key words. supernovae: general – stars: evolution – surveys

1. Introduction

The rate of supernova explosions is astrophysically important because it determines the rate at which heavy elements are dispersed into the interstellar medium, thereby constraining galactic chemical evolution. Since the progenitors of core-collapse supernovae (SNcc) are believed to be short-lived massive stars, the SNcc rate is expected to reflect the star-formation rate, increasing with redshift like $\sim(1+z)^{3.6}$ for $z < 0.5$ (Hopkins & Beacom 2006). Thermonuclear type Ia supernovae (SNIa) have both long- and short-lived progenitors so the SNIa rate has a delayed component making the SNIa rate rise more slowly with redshift, $\sim(1+z)^2$ (Pritchet et al. 2008).

The SNIa rate is now known to a precision of about 20%. Measurements have profited from the high luminosity of SNIa which make them relatively easy to detect and identify. Furthermore, their utility as cosmological distance indicators has motivated intense searches. An example is the Supernova Legacy Survey (SNLS) at the Canada-France-Hawaii Telescope (CFHT) performed between 2003 and 2008. Using early SNLS data, Neill et al. (2006) derived a SNIa rate at a redshift $z \sim 0.5$ of

$$\frac{R_{\rm Ia}(z=0.5)}{10^{-4}\ {\rm yr}^{-1}(h_{70}^{-1}\ {\rm Mpc})^{-3}} = 0.42 \pm 0.06(stat.)^{+0.13}_{-0.09}(syst.)$$

where $h_{70} = H_0/70\ {\rm km\,s^{-1}\ Mpc^{-1}}$.

The rate for SNcc is more difficult to measure because observed SNcc have a magnitude distribution that peaks roughly 1.5 mag fainter than SNIa and covers a range of more than 5 mag (Richardson et al. 2002). The local rate was measured by Cappellaro et al. (1999) using 137 supernovae discovered by eye and photographically. Most had spectroscopic identification, about half being SNIa and half SNcc (SNIb/c and SNII). After efficiency corrections, the SNcc rate was found to be a factor 2.4 ± 1.3 greater than the SNIa rate.

The SNcc rate at $z \sim 0.3$ was measured by Cappellaro et al. (2005) and more recently by Botticella et al. (2008). The latter used images taken over a six year period with typically four months between images. They found 18 SNcc candidates and 13 SNIa candidates (of which a total of 25 are spectroscopically confirmed) to find a SNcc rate at $z \sim 0.26$ a factor 4 ± 2 greater than the SNIa rate. Finally, Dahlen et al. (2004) used the Advanced Camera for Surveys on the Hubble Space Telescope to obtain images for five epochs separated by ~45 days. For redshifts <1, they found 17 SNIa candidates (with some spectroscopic identification) and 16 SNcc candidates (no spectroscopic identification) which allowed them to derive $R_{\rm cc}/R_{\rm Ia} = 3.6 \pm 2.0$ at $z \sim 0.4$ and $R_{\rm cc}/R_{\rm Ia} = 2.5 \pm 1.0$ at $z \sim 0.8$.

All existing measurements of the SNcc rate suffer from the fact that the discovery procedure involved the comparison of images separated in time by intervals comparable to or greater

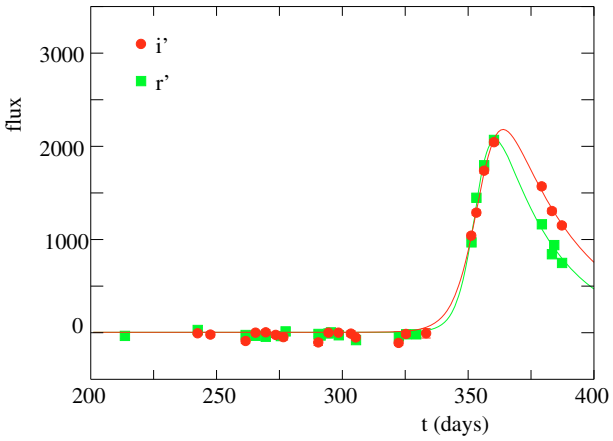

Fig. 1. The r' and i' light curves of a SNIa. The spectroscopic redshift is 0.332, the host photometric redshift 0.294, and the peak magnitude $i' = 21.6$. The time corresponds to MJD-52 640.

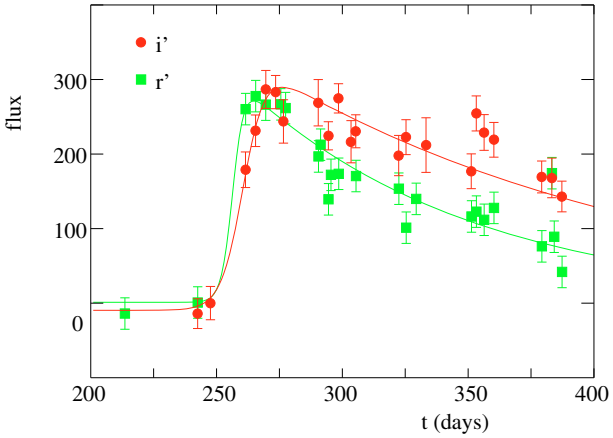

Fig. 2. The r' and i' light curves of a SNIIp. The spectroscopic redshift is 0.328, the host photometric redshift 0.335, and the peak magnitude $i' = 23.8$. The time corresponds to MJD-52 640.

than the characteristic ∼1 month time scales of supernovae. Consequently, well-sampled light curves for most candidates are not available, complicating the type identification and efficiency calculations. The SNLS "rolling search" avoids this problem because of its high cadence monitoring of four 1 deg^2 fields in the g', r', i' and z' bands over a total of 5 years. During each 6 month observing season for each field, typically four observations per lunation were obtained in the r' and i' bands, three in the z' band and two in the g' band. This strategy yields well-sampled light curves (e.g. Figs. 1–3) with high efficiency for all events occurring during the observing season and having maximum fluxes brighter than $i' \sim 24$. This makes the sample of normal SNIa essentially complete up to $z = 0.6$. For the fainter SNcc, SNLS effectively monitors a volume that is a calculable function of the apparent magnitude and redshift. This will allow us to derive the differential supernova rate (rate per absolute magnitude interval) for supernova with redshifts <0.4 and within 4.5 mag of normal SNIa.

The primary goal of SNLS was cosmology with SNIa. As such, mostly SNIa-like objects were targeted for spectroscopy (Sullivan et al. 2006) and the majority of our SN candidates do not have spectroscopic identification or redshifts. We therefore used host photometric redshifts for this study though we are in the process of obtaining host spectroscopic redshifts. For supernovae without spectroscopic identification, knowledge of the

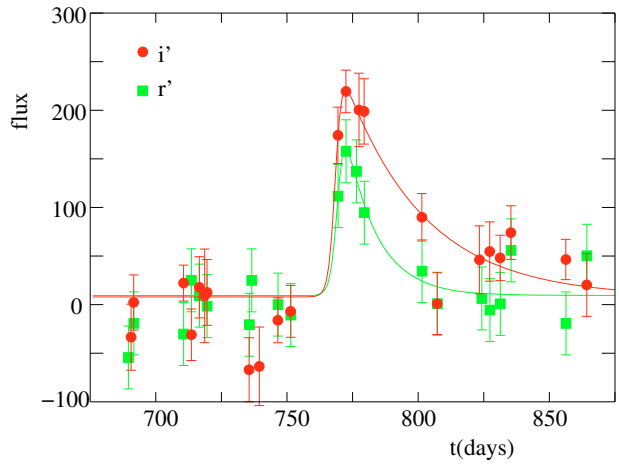

Fig. 3. The r' and i' light curves of a SNcc candidate. The host photometric redshift is 0.36 and the peak magniude $i' = 24.1$. It is the faintest event used here to measure the core-collapse rate. The time corresponds to MJD-52 640.

host redshift allows us to determine if the supernova four-band light-curves are consistent with the family of light curves typical of SNIa. The combination of spectroscopic and photometric typing will allow us to identify most SNIa. A relatively uncontaminated sample of SNcc is then defined as those supernovae not identified as SNIa. Use of the previously measured SNIa rate (Neill et al. 2006) will then allow us to derive the SNcc rate. The measurement will use only supernovae with redshifts <0.4, beyond which the efficiency for detecting SNcc is too small to add significantly to the sample. This has the additional advantage that in this redshift range, the 615 nm Si II absorption feature is visible simplifying spectroscopic identification of SNIa.

The outline of this paper is as follows. Section 2 presents the light curve construction and event selection. Section 3 presents the characteristics of the supernova candidates. Section 4 defines the SNIa and SNcc candidate samples. Section 5 derives the relative SNIa and SNcc rates from which we deduce the SNcc rate. Section 6 concludes with a comparison of previous results.

Throughout, magnitudes are expressed in the AB system (Fukugita et al. 1996). A flat ΛCDM universe with $\Omega_M = 0.27$ is assumed.

2. Event selection

For this study, we performed a "deferred" search for transient events that was completely independent of the real-time search[1] used to select supernovae for spectroscopy targets and for subsequent use in cosmological parameter analyzes. The details of the deferred search are given elsewhere (Bazin 2008; Bazin et al. 2009). We used SNLS observations of the four "deep" fields (D1, D2, D3, D4) from January 1st, 2003 to September 21, 2006. A reference image for each field and filter was constructed by co-adding the images from 20 good quality nights. The reference image was then subtracted from all science images of the same field and filter (after seeing-adjustment). In the i' filter, the subtracted images from each lunation were combined to form one "stacked" image per lunation and stellar objects were searched for on each of these stacks. Approximately 300 000 objects were found, mostly spurious detections due to saturated signals from bright objects. Four-filter light curves for these objects were then

[1] http://legacy.astro.utoronto.ca/

obtained from individual subtracted images by differential photometry with PSF fitting, imposing the position found on the i' stack. Fluxes were calibrated using the set of SNLS tertiary standards (Astier et al. 2006).

The event selection criteria applied on the detected light curves are described in detail in Bazin et al. (2009). Spurious detections were mostly eliminated by requiring that the light curves in i' and r' have at least three successive photometric points with fluxes above 1σ from base line and their dates of maximum flux should be within 50 days from each other. Light curves corresponding to detections near stars as identified in our reference images were also discarded. Accepted light curves were fit with the phenomenological form

$$f(t) = A\frac{e^{-(t-t_0)/\tau_{\rm fall}}}{1+e^{(t-t_0)/\tau_{\rm rise}}} + B \quad (1)$$

while this form has no particular physical motivation, it is sufficiently general to fit the shape of all types of supernovae. Long-term variable objects (such as AGNs) were rejected by comparing the χ^2 of the light curve fit using (1) with fits to a constant flux, and only accepting objects for which the phenomenological model is a substantially better fit. In addition, we require that the light-curve be consistent with a time-independent flux before and after the main variation as fitted by (1). The precise cuts were defined with the help of synthetic SNIa light curves and selected real light curves which have been confirmed by spectroscopy as type Ia or core-collapse SNe. Finally, good time sampling criteria were applied, i.e. requiring at least one pre-max epoch within 30 days and one post-max epoch within 60 days of the date of maximum flux in the i' and r' filters, and at least two epochs in that time interval in the g' and z' filters. A set of 1462 events was thus retained.

Light-curves for three events are shown in Figs. 1–3. The first shows a typical spectroscopically-confirmed SNIa with spectroscopic redshift $z = 0.332$ and the second a typical spectroscopically-confirmed SNcc with spectroscopic redshift $z = 0.328$. The third is one of the faintest events to be used in Sect. 5 to measure the core-collapse rate. Its peak magnitude is $i' = 24.1$, as fitted by (1).

To identify host galaxies for the events, we used the photometric galaxy catalog of Ilbert et al. (2006). The host for an event was chosen to be the galaxy with the smallest distance, r, between the event and the galaxy center in units of the galaxy's effective radius, $r_{\rm gal}$, defined as the half-width of the galaxy in the direction of the event. The value of $r_{\rm gal}$ was defined by the A, B and θ SExtractor parameters (Bertin & Arnouts 1996). The match was considered successful if the host was at a distance $r < 5r_{\rm gal}$. This choice was a compromise between host finding efficiency and accidental mismatching. Of the 1462 selected events, 1329 (91%) have matched hosts and of these 1207 (91%) have a photometric redshift. Figure 4 shows the host spectroscopic redshift vs. photometric redshift (Ilbert et al. 2006) for events with both. After elimination of outliers, the deduced resolution for photometric redshifts is $\sigma_z \sim 0.04$ for $z < 0.4$.

For the SNcc rate measurements, we will consider only the 239 events with $z_{\rm host} < 0.4$. These light curves were visually scanned in order to eliminate a few residual non-SN events. Six light curves were clear physical variable events, varying on a time-scale consistent with that of SNe but their light curves showed other details incompatible with that hypothesis (no flux in g', r', z' filter or rise time longer than fall time). Another 12 events had light curves with very low maximum flux and erratic variations and thus most probably residual noise events

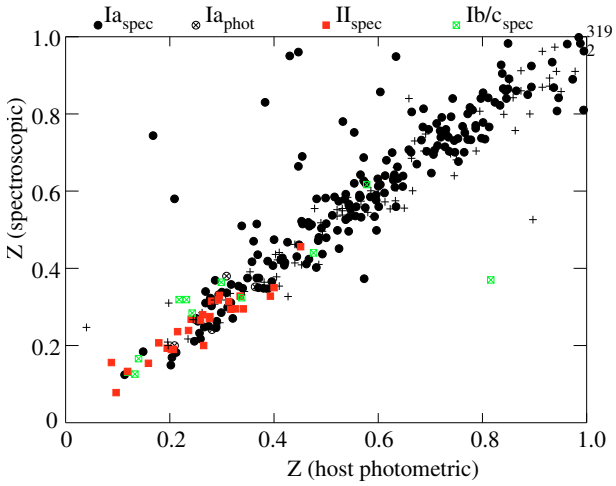

Fig. 4. SNLS spectroscopic redshifts vs. host photometric redshifts taken from the catalog of Ilbert et al. (2006). Spectroscopically identified supernovae and photometrically identified SNIa are marked by the signs defined at the top of the figure. The crosses are supernovae whose type is not determined spectroscopically or photometrically.

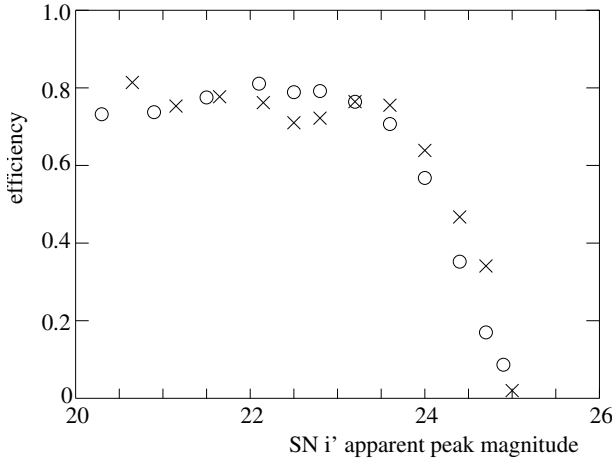

Fig. 5. Pre-selection efficiency as a function of i'. The "efficiency" is defined as the number of reconstructed events in a given magnitude interval divided by the number of generated events in the same interval. The circles are for SNIa and the crosses for SNcc with $\tau_{\rm fall} = 100$ days.

which appear to be associated with low redshift galaxies. After elimination of these events, we were left with 221 events.

The efficiency of the event selection procedure was calculated by treating simulated supernovae with the same procedure. Supernovae added to real i'-band images were used to test the initial detection stage in i'. The efficiency of the subsequent event selection cuts was calculated by applying them to light curves generated by a Monte-Carlo simulation that takes into account the photometric resolution and the observing sequence. The resulting efficiency is a function of the maximum fluxes in the four bands and the associated time scales. However, to good approximation the efficiency is simply a function of the maximum in the i' band. The efficiency is shown in Fig. 5 for SNIa and for long SNcc ($\tau_{\rm fall} = 100$ days). In both cases, the efficiency is relatively i'-independent at a value of ~0.8 for $i' < 23$ at which point it starts to decline, reaching 0.4 at $i' = 24.3$.

The performance of our selection pipeline was checked by comparing it with the results of the SNLS real-time pipeline used to select spectroscopy targets. A total of 340 supernovae were targeted during the period considered here including events

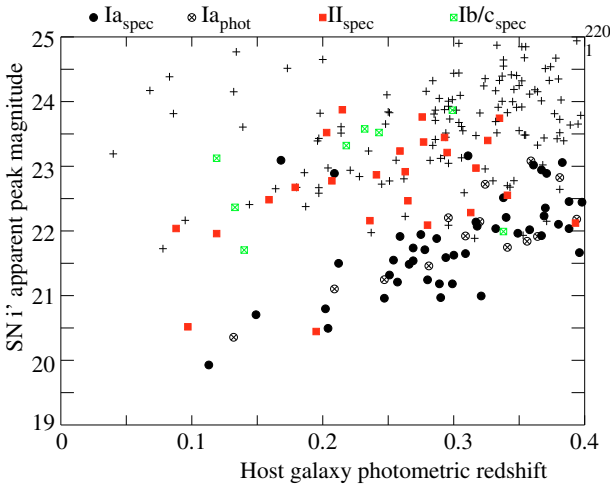

Fig. 6. The peak i' magnitude vs. host photometric redshift. Spectroscopically identified supernovae and photometrically identified SNIa are marked by the signs defined at the top of the figure. Events without such identification (crosses) are SNcc candidates without spectroscopic confirmation. Most identified SNIa lie in the band with $i' \sim 21.8 + 5\log(z/0.3)$. Note that the two anomalously faint spectroscopically confirmed SNIa at $z \sim 0.17$ and $z \sim 0.21$ are the corresponding outliers in Fig. 4 indicating an incorrect host-photometric redshift.

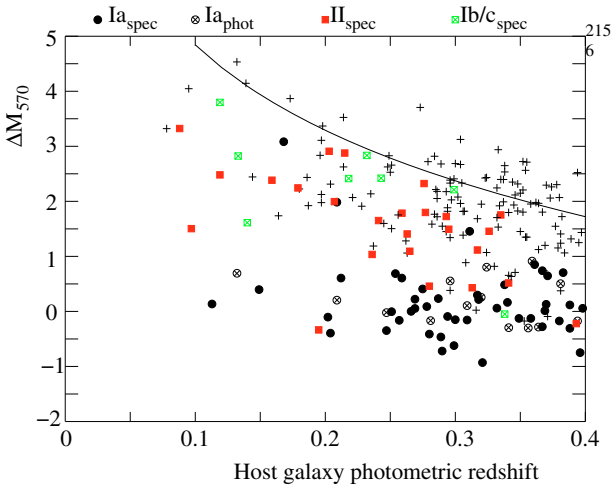

Fig. 7. The pseudo-absolute magnitude ΔM_{570} defined by (3) as a function of redshift. Identified SNIa are concentrated near $\Delta M_{570} = 0$. The line in the upper-right corresponds to the $m_{570} = 24.1$. Spectroscopically identified supernovae and photometrically identified SNIa are marked by the signs defined at the top of the figure.

as faint as $i' = 24.4$. Of these, all but two were found on the i' stacked images. (The two lost events were outside the reference images.) Of the 338 events, 295 passed our selection criteria. The loss of the 43 events was due to our time sampling criteria which is more restrictive than the real-time criteria.

3. Event characteristics

Figure 6 shows the i' Hubble diagram for the 221 events with host photometric redshifts <0.4. Events that are spectroscopically identified as SNIa or SNcc (SNII, SNIb, SNIc) are marked. Also marked are photometrically identified SNIa as discussed in Sect. 4. The spectroscopic SNIa's fall mostly along the band of bright events centered approximately on $i' \sim 21.8 + 5\log(z/0.3)$. The spectroscopic SNcc's are generally fainter with $i' > 22.7 + 5\log(z/0.3)$.

The supernovae that we will use to measure rates have a wide range of redshifts up to $z = 0.4$. In order to compare supernovae of differing z, we define an AB magnitude centered on 570 nm in the supernova rest-frame by a simple redshift-dependent interpolation between r' and i':

$$m_{570} \equiv (4z - 0.4)i' + (1.4 - 4z)r'. \quad (2)$$

This gives $m_{570}(z = 0.1) = r'$ ($\lambda = 626$ nm) and $m_{570}(z = 0.35) = i'$ ($\lambda = 769$ nm). We then define the quantity ΔM_{570} to be proportional to the absolute magnitude taking into account the supernova distance but not host absorption:

$$\Delta M_{570} \equiv m_{570} - 2.5\log\left[(1+z)d(z)^2\right] - C \quad (3)$$

where

$$\mathrm{d}(z) = \int_0^z \frac{\mathrm{d}z'}{\sqrt{\Omega_\mathrm{m}(1+z')^3 + (1-\Omega_\mathrm{m})}} = \frac{d_\mathrm{L}}{(c/H_0)(1+z)}. \quad (4)$$

The constant $C = 24.2$ is chosen so that the spectroscopically confirmed SNIa are centered on $\Delta M_{570} = 0$.

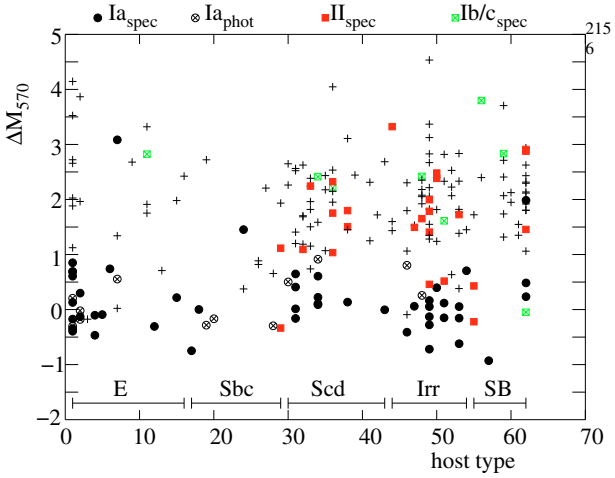

Fig. 8. Host morphological type as a function of ΔM_{570}. The types are derived from the best spectral templates of Ilbert et al. (2006). Spectroscopically identified supernovae and photometrically identified SNIa are marked by the signs defined at the top of the figure.

Figure 7 shows ΔM_{570} as a function of redshift. The spectroscopically identified SNIa and SNcc are now separated horizontally with $\Delta M_{570} < 0.75$ dominated by SNIa and $\Delta M_{570} > 0.75$ containing most spectroscopically-confirmed SNcc. The characteristics of the events as a function of ΔM_{570}, shown in Figs. 8–10, are broadly consistent with those expected for SNIa and SNcc. Figure 8 shows ΔM_{570} as a function of the photometric host types (Ilbert et al. 2006). As expected for a sample dominated by SNcc, the faint events have relatively fewer early-type hosts (19/152) compared to 24/69 for the bright events. Figure 9 shows ΔM_{570} as a function of $\tau_\mathrm{fall}/(1+z)$. As with low redshift SNcc (Richardson et al. 2002), about half (47/108) the faint events have $\tau_\mathrm{fall}/(1+z) > 50$ days, characteristic of plateau SNII and significantly longer than fall times for SNIa, $20 < \tau_\mathrm{fall}/(1+z) < 30$ days. Finally, Fig. 10 shows the color–magnitude diagram using the *AB* magnitude at 450 nm in the rest frame:

$$m_{450} \equiv (4z - 0.4)r' + (1.4 - 4z)g'. \quad (5)$$

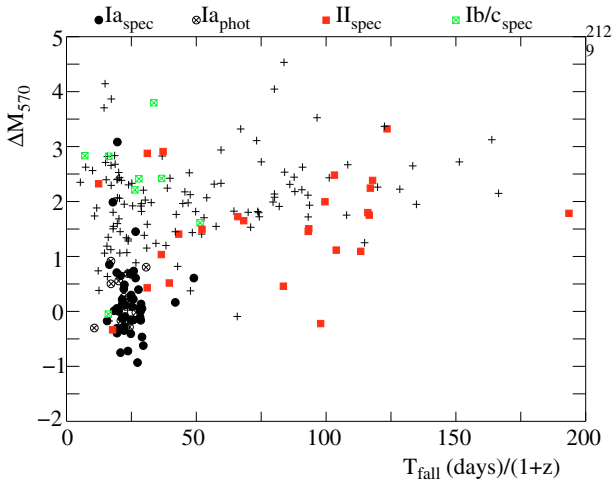

Fig. 9. Fall time $\tau_{\rm fall}/(1+z)$ (i' band) as a function of ΔM_{570}. Spectroscopically identified supernovae and photometrically identified SNIa are marked by the signs defined at the top of the figure.

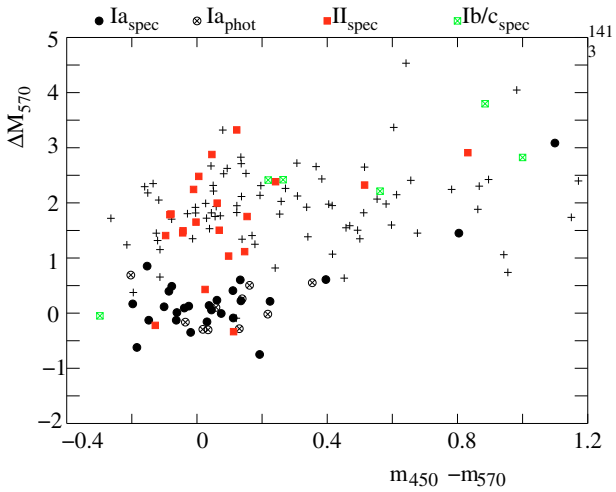

Fig. 10. The color–magnitude diagram. Only the subset of events with points in g' near maximum light appear in the plot. Spectroscopically identified supernovae and photometrically identified SNIa are marked by the signs defined at the top of the figure.

The SNIa candidates have a narrower color distribution than the SNcc candidates.

4. Supernova classification

SNLS did not have sufficient telescope time to obtain spectra of all SNIa candidates. Therefore, in order to define a more complete SNIa sample, the four-band light curves of all events were compared to SALT2 SNIa template light curves (Guy et al. 2007). The SALT2 model characterizes light curves by four parameters: the date of maximum in the rest-frame B-band, the maximum flux in the rest-frame B band, a "color" parameter roughly equivalent to rest-frame $B-V$, and a "stretch" parameter that dilates the event time scale. The light curves were fit for these parameters imposing the host photometric redshift. Events were "photometrically" classified as SNIa if the four-band fit was reasonable (χ^2/d.o.f. $<$ 10) and if fit parameters corresponded to normal SNIa. In particular, cuts were applied to the rise and fall times, the color, c, and to the position in the two color magnitude diagrams, $(g'-i')$ vs. g' and $(r'-z')$ vs. z'.

Table 1. The numbers of events for each spectroscopic and photometric classification.

	Photometric classification	
Spectroscopic classification	SNIa	not SNIa
SNIa	39	7
ambiguous	4	24
no spectrum	10	69
SNcc	1	23

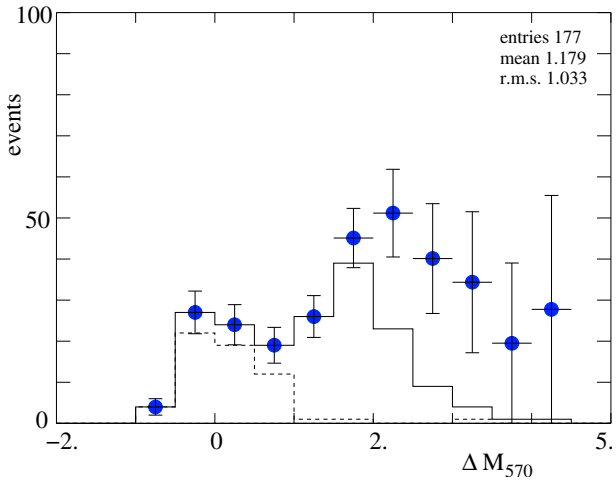

Fig. 11. The distribution of ΔM_{570}. The solid histogram shows the distribution of ΔM_{570} for events with $m_{570} < 24.1$ and $0.05 < z < 0.4$. The dashed histogram shows the distribution for spectroscopically and photometrically selected SNIa. The data points with error bars show the number of events after correction for the detection efficiency and the dependence of the survey volume on ΔM_{570}.

Table 1 shows the number of events photometrically classified as SNIa or "not SNIa" for events classified spectroscopicaly as SNIa, SNcc and "ambiguous", as well as for events for which no spectrum was obtained. The table contains only those events that will be used for rate measurements in the next section, i.e. those with $0.05 < z < 0.4$ and $m_{570} < 24.1$ (Eq. (2)). The reasonable performance of the photometric classification is demonstrated by the fact that only seven of the 46 spectroscopic SNIa were not selected and only one of the 24 spectroscopic SNcc was selected. The photometric classification also selected 14 events that had not been classified spectroscopically as SNIa. As detailed below, the lack of spectroscopic confirmation was generally due to an insufficient supernova signal over the galactic background or to lack of telescope time to obtain a spectrum.

As our nominal SNIa sample, we choose the 46 events that were spectroscopically identified as SNIa plus the 14 events photometrically identified as SNIa that were not spectroscopic SNcc. The nominal SNcc sample is the 117 remaining events. The distribution of ΔM_{570} for these events are shown as the histograms in Figs. 11 and 12.

We have no evidence that the 60 SNIa candidates are contaminated with SNcc incorrectly identified as SNIa. We first consider the 46 spectroscopically identified SNIa. It is unlikely that these events are significantly contaminated with SNcc since for $z < 0.4$ the Si(615 nm) line is visible making the identification reliable. In fact, of the 46 events, 43 were classified spectroscopically as "SNIa" and only 3 as "SNIa?". The three "SNIa?" events are all selected photometrically making them good SNIa candidates. Of the 46 events, only seven were not photometrically accepted but for reasons that do not call into question their SNIa

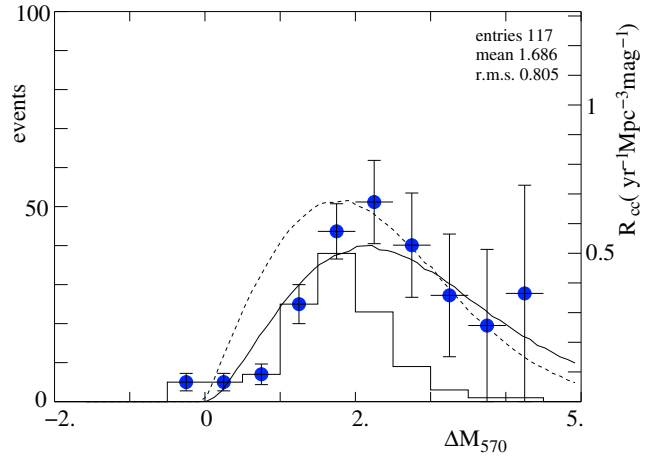

Fig. 12. The differential SNcc rate. The data points are those of Fig. 11 with the SNIa subtracted (statistical errors only). The left-hand scale is the number of events and the right-hand scale is the absolute differential rate derived from the total rate in Sect. 5. The dashed curve shows the intrinsic distribution for a toy model (of no physical motivation) with rate $\propto \Delta M_{570} \exp[-(\Delta M_{570}/2.5)^2]$ while the solid line shows the distribution for this model after including the host absorption predicted by the model of Hatano et al. (1998).

character: three had photometric redshifts significantly different from the spectroscopic redshifts causing the SALT fit to be very poor; one event had an extreme color parameter falling outside our cuts; three events had a small number of poor photometric points causing the fits to fail our χ^2 cut.

We now consider contamination of the 14 SNIa that have only photometric confirmation. Of these, four events have spectroscopy that was of insufficient signal-to-noise to determine the SN type. The remaining 10 events had no spectra either because the event was discovered too late or because the estimated signal-to-noise was insufficiently (local flux increase <20%). Only one of the 14 events was judged "unlikely" to be a SNIa by the spectroscopy target selection group, but the full light curve indicates that it is consistent with being a normal SNIa. We therefore have no evidence that the 14 events are contaminated with SNcc. However, we have no good template catalog of bright SNcc to evaluate the probability that a bright SNcc passes our SNIa photometric selection. We therefore conservatively assign a systematic one standard deviation upper limit of 7 events to contamination of the SNIa sample with SNcc.

While we have no evidence that the SNIa sample is contaminated with SNcc, it is certain that the SNcc sample is contaminated by sub-luminous SNIa. We will evaluate this contamination in the next section.

5. The core-collapse rate

In this section, we will derive the SNcc rate using events with $0.05 < z < 0.4$ and $m_{570} < 24.1$. The cut on m_{570} is used to ensure that only events with good detection efficiency are used. The requirement that $z > 0.05$ eliminates one event at $z = 0.04$. The uncertainty in ΔM_{570} is $\sigma(\Delta M_{570}) \sim 2\sigma_z/z$ so the event with $z = 0.04$ has $\sigma(\Delta M_{570}) > 1$ and we prefer to eliminate it. (In fact, this event is a spectroscopic outlier with $z_{\rm spec} = 0.247$.) With the m_{570} and redshift cuts, we are left with 177 events, 60 of which are spectroscopically or photometrically identified SNIa.

From these numbers, we will derive the SNcc rate as follows. We first assign weights to the observed events that take into account detection efficiency and the volume over which the event could be detected by SNLS. Because of their intrinsic faintness, this will significantly increase the number of SNcc candidates to 287. We next evaluate two effects that can change the number of SNcc candidates relative to SNIa candidates. The first is simple spectral or photometric misidentification. The second comes from the use of host photometric redshifts which, we will see, has a slight tendency to increase the number of SNIa candidates relative to SNcc candidates. Using the corrected number of candidates, we then calculate the SNcc rate relative to the SNIa rate. By adopting the previously measured SNIa rate, we then derive the SNcc rate for luminosities within 4.5 mag of normal SNIa. Finally, we estimate the total SNcc rate taking into account the decrease in the number of observed supernovae due to extinction by dust in the host galaxy.

5.1. Event weights

The observed distribution of ΔM_{570} is the histogram shown in Fig. 11 for the 177 events with $z < 0.4$ and $m_{570} < 24.1$. In order to derive the true distribution of ΔM_{570} for events with $z < 0.4$, this distribution must be corrected for the i'-dependent detection efficiency and, more importantly, for the fact that an event with absolute magnitude ΔM_{570} can be seen only up to a redshift, $z_{\rm max}$ defined by

$$\sqrt{1+z_{\rm max}}\, d(z_{\rm max}) = 10^{0.2(m_{570\ \rm max} - C - \Delta M_{570})} \quad (6)$$

where $d(z)$ is defined by (4) and $m_{570\ \rm max} = 24.1$ is the maximum accepted magnitude. Events with $z_{\rm max} < 0.4$ (i.e. $\Delta M_{570} > 1.7$) must be given a weight, $W > 1$. The weight takes into account, most importantly, the fact that SNLS detects them over a smaller volume. Of secondary but non negligible importance is the fact that the SNcc rate is believed to increase with redshift, $R_{\rm cc} \propto (1+z)^{\alpha}$ with $\alpha \sim 3.6$ to reflect the increasing star-formation rate with redshift. We are therefore sensitive to intrinsically faint supernovae only in a redshift range where rate is small. We correct for this with $\alpha = 3.6$ appropriate for SNcc because our SNIa candidates are all bright enough to have $z_{\rm max} > 0.4$. Finally, because of cosmological time dilation, the SNLS observing time is proportional to $(1+z)^{-1}$. The total weight, $W(\Delta M_{570}, i')$, is therefore given by

$$W^{-1} \propto \frac{\epsilon(i')}{\epsilon(i'=21)} \int_0^{z_{\rm max}} \frac{{\rm d}z'{\rm d}(z')^2(1+z')^{\alpha-1}}{\sqrt{\Omega_{\rm m}(1+z')^3 + (1-\Omega_{\rm m})}}, \quad (7)$$

where $\epsilon(i')$ is the event detection efficiency. The factor of proportionality is chosen so that $W(z_{\rm max} = 0.4, i' = 21) = 1$. Without the factors of $(1+z)$ in (4) and (7), the weight would be simply the product of $\epsilon(i'=21)/\epsilon(i')$ and the euclidean volume ratio $(0.4/z_{\rm max})^3$. The factors of $(1+z)$ correct for the redshift evolution of the volume element, the exposure time, and the SNcc rate.

Weighting individual events gives the corrected ΔM_{570} distribution shown by the data points and error bars in Fig. 11. All of the 60 SNIa candidates have weights near unity. Because of their faintness, many of the 117 SNcc candidates have $W > 1$ and the corrected number of SNcc candidates is 287 ± 40 (statistical error only).

5.2. Corrections for misidentification and redshift migration

In this section we correct the raw number of SNIa and SNcc candidates for two effects that can affect their numbers: type misidentification (summarized in Table 2) and redshift migration due to the use of photometric redshifts.

Table 2. Corrections applied to the 60 SNIa candidates and 287 (weighted) SNcc candidates.

Correction	SNIa	SNcc
SNIa incorrectly identified as SNcc		
sub-luminous SNIa	$+9 \pm 5$	-9 ± 5
normal SNIa	$+2 \pm 1$	-2 ± 1
SNcc incorrectly identified as SNIa	0^{+0}_{-7}	0^{+7}_{-0}
Contamination by non-SN	0 ± 0	0^{+0}_{-4}
Total	$+11^{+5}_{-9}$	-11^{+9}_{-7}

The first shift in the SNIa-SNcc ratio is due to SNIa that are incorrectly identified as SNcc. We divided this correction into that for "sub-luminous" SNIa and normal SNIa. Sub-luminous SNIa (Li et al. 2001) have a mean magnitude 1.5 mag below the mean magnitude for normal SNIa and account for $16 \pm 6\%$ of SNIa. None are found in our sample since both selection for spectroscopy and photometric selection aimed at finding normal SNIa. We therefore add (subtract) 9 ± 5 events to the SNIa (from the SNcc) samples. For normal SNIa, we must correct for events that were neither spectroscopically nor photometrically selected. From Table 1, of the 46 spectroscopically confirmed events, only 7 were not photometrically selected. This gives an inefficiency of $7/46 = 0.15$ for photometric identification of spectroscopically confirmed SNIa. To the 14 SNIa candidates relying solely on photometric selection, we can therefore add $0.15 \times 14 = 2$ events and subtract the same number from the SNcc.

As discussed in Sect. 4, we make no correction for SNcc incorrectly identified as SNIa but assign a systematic one standard deviation upper limit of 7 events to contamination of the SNIa sample with SNcc.

Contamination with non-supernova events is expected to be unimportant. The scan of events resulted in the elimination of only six AGN-like events and the identification of four additional events that were judged uncertain. We adopt four events as our one standard deviation upper limit on AGN contamination of the SNcc sample.

Finally, we correct for redshift migration (Eddington bias), an effect that comes from our use of photometric redshifts with a modest resolution of $\sigma_z \sim 0.04$. Because there are more supernovae at high redshift than at low redshift, the main effect of this resolution is for high redshift supernovae to migrate below the $z = 0.4$ cutoff. If there were no cut $m_{570} < 24.1$, this would increase the number of SNIa and SNcc candidates by the same factor. The fact that SNcc are fainter than SNIa means that migrating SNcc are less likely to satisfy $m_{570} < 24.1$ than migrating SNIa. We have used a Monte Carlo simulation to estimate this effect. The simulation generates events with a realistic redshift and M_{570} distribution and uses the observed spectroscopic-photometric redshift pairs from Fig. 4 to assign photometric redshifts. Outliers in this plot are used so the simulation takes into account catastrophic redshifts. Counting weighted simulated events indicates that the migration makes the measured SNcc-SNIa rate ratio $(15 \pm 4)\%$ less than the real rate ratio. The statistical error comes from the limited number of redshift pairs we have used for the simulation. The measured SNcc-SNIa rate will therefore be multiplied by a factor 1.15 to take into account this effect.

5.3. The SNcc-SNIa relative rate

The corrections for the number of events shown in Table 2 give an increase of 11^{+5}_{-9} SNIa candidates, and a corresponding decrease in the number of SNcc candidates. The corrected relative rate for $z < 0.4$ is therefore

$$\frac{R_{\rm cc}(\Delta M_{570} < 4.5)}{R_{\rm Ia}} = \frac{287 - 11}{60 + 11} \times 1.15 = 4.5 \pm 0.8(stat.)^{+0.9}_{-0.7}(sys.),$$

where the factor 1.15 takes into account redshift migration. The ratio is for $z < 0.4$ corresponding to an expected mean redshift of 0.306 for a rate proportional to $(1 + z)^2$ and a mean of 0.313 for a rate proportional to $(1 + z)^{3.6}$. Our sample of 60 SNIa has a mean redshift of 0.30 ± 0.01, consistent with expectations for a complete (volume limited) sample.

The systematic error in $R_{\rm cc}/R_{\rm Ia}$ includes those due to the corrections from the previous section as well as three additional systematic uncertainties which we add in quadrature.

The first additional systematic concerns the uncertainty in the relative efficiencies for SNIa and the fainter SNcc. To avoid large uncertainties, we have used only events with $m_{570} < 24.1$ where the efficiency is high. With this cut, there is only a 10% difference in the SNcc rate calculated with the nominal efficiencies and that calculated assuming a magnitude-independent efficiency. We adopt 10% as the nominal systematic error from this source. To check that there is no significant uncorrected event loss near the magnitude cut, we verified that the derived SNcc rate does not depend significantly on the position of the magnitude cut. For example, using $m_{570\,\rm max} = 23.6$, the number of events SNcc candidates is reduced from 117 to 82. After weighting, this is increased to 334 ± 80 consistent with the 287 ± 45 event found using $m_{570\,\rm max} = 24.1$. (Most of the increase comes from the two events with $\Delta M_{570} > 3.5$ which are given greater weights with $m_{570\,\rm max} = 23.6$.)

The second systematic concerns the star-formation rate. The corrected differential rate was calculated assuming that the SNcc rate is proportional to $(1+z)^\alpha$ with $\alpha = 3.6$ according to Hopkins & Beacom (2006). These authors do not cite an uncertainty for α but inspection of the data indicates that $\alpha = 3.6 \pm 1.0$ is reasonable. This corresponds to a 10% systematic uncertainty in the SNcc rate.

The final systematic concerns our requirement that a host galaxy be found and that a redshift be given in the Ilbert et al. (2006) catalog. This requirement could conceivably favor SNcc or SNIa. For spectroscopically identified supernovae with $z < 0.4$, a host galaxy is generally found but a redshift may not be given in the catalog. For 41 spectroscopic SNIa with spectroscopic redshifts <0.4 that were found in the deferred search, only 4 have no host redshift while for the 36 spectroscopic SNcc there are only 3 with no host redshift. Thus, we see no difference in host-redshift measurement efficiency at the 5% level and we adopt this as the systematic uncertainty.

5.4. The SNcc rate

To derive a value of $R_{\rm cc}$ we adopt the value of $R_{\rm Ia}$ measured by Neill et al. (2006) at $z = 0.5$: 0.42×10^{-4} yr$^{-1}(h_{70}^{-1}$ Mpc$)^{-3}$ Our measurement of $R_{\rm cc}/R_{\rm Ia}$ is effectively at $z = 0.3$ and we adopt a SNIa rate at this redshift of 0.315×10^{-4} yr$^{-1}(h_{70}^{-1}$ Mpc$)^{-3}$ calculated assuming $R_{\rm Ia} \propto (1+z)^2$. This gives a SNcc rate within 4.5 mag of normal SNIa of

$$\frac{R_{\rm cc}(\Delta M_{570} < 4.5)}{10^{-4}\ {\rm yr}^{-1}(h_{70}^{-1}\ {\rm Mpc})^{-3}} = 1.42 \pm 0.30\,(stat.)^{+0.32}_{-0.24}\,(sys.)$$

we have added the statistical and systematic uncertainties of $R_{\rm cc}/R_{\rm Ia}$ and of $R_{\rm Ia}$ separately in quadrature though not including

the systematic uncertainty in $R_{\rm Ia}$ due to sub-luminous and absorbed supernovae because it is already included in the uncertainty in $R_{\rm cc}/R_{\rm Ia}$.

With the determination of the total SNcc rate, we can give an absolute differential rate per unit magnitude for SNcc. It is shown as the right-hand scale in Fig. 12. The rate is measured down to luminosities 4.5 mag fainter than normal SNIa. It should however be emphasized that there are only two events with $\Delta M_{570} > 3.5$. One of them has spectroscopic confirmation and the spectroscopic redshift, $z = 0.131$, is in good agreement with the host photometric redshift, $z = 0.119$. The other event has a host spectroscopic redshift[2] $z = 0.0815$ in good agreement with the host photometric redshift used here, $z = 0.095$. Thus, we have no indication that these two events are higher luminosity events that have migrated from high redshift.

To estimate a *total* rate for SNcc we need to estimate the number of SNcc with $\Delta M_{570} > 4.5$ either because they are intrinsically faint (e.g. SN1987A, $\Delta M_{570} \sim 5.5$) or because of high host extinction. SNLS obviously cannot say anything about intrinsically faint supernovae. However, by adopting a host galaxy extinction model, we can estimate the number of SNcc that have intrinsic luminosities within our range of sensitivity but that are lost because of high host extinction. We have used the results of Hatano et al. (1998) who give (their Table 1 and Fig. 1) the distribution of A_B as a function of host inclination angle. This can be converted to a distribution of absorption at 570 nm and convoluted with the pre-absorption distribution of M_{570}. For example, if we model the intrinsic SNcc magnitude distribution shown as the dashed line in Fig. 12, then the SNcc host extinction model of Hatano et al. (1998) predicts the distribution shown by the solid line in the figure. With this model, 15% of SNcc have $\Delta M_{570} > 4.5$. Our estimated total rate is then increased to $R_{\rm cc} = 1.63 \times 10^{-4}$ yr$^{-1}(h_{70}^{-1}$ Mpc$)^{-3}$. In our model, most of the events with $\Delta M_{570} > 4.5$ are highly absorbed so our estimate should be considered a lower limit on the SNcc rate that ignores supernovae that are intrinsically fainter than $\Delta M_{570} = 4.5$.

6. Discussion

Figure 13 summarizes the published measurement of the SNcc rate. All data is consistent with a rate that increases with redshift like the $SFR \propto (1+z)^{3.6}$. It should be emphasized that the previous measurements use quite different detection and analysis procedures. We therefore refrain from drawing any quantitative conclusions about the redshift dependence of the SNcc rate.

Our results will be improved in the future with the addition of two more years of SNLS data, and with the use of host spectroscopic redshifts that we are in the process of obtaining.

Acknowledgements. The SNLS collaboration gratefully acknowledges the assistance of Pierre Martin and the CFHT Queued Service Observations team.

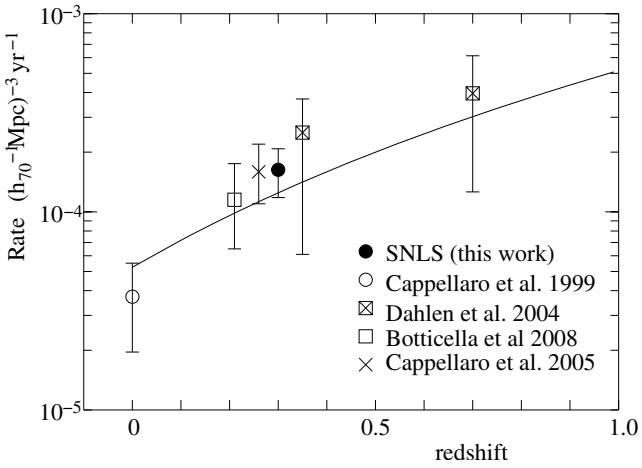

Fig. 13. The measured rate of SNcc as a function of redshift. The SNLS point includes a 15% correction for host absorption as described in the text. The error bars correspond to statistical and systematic uncertainties added in quadrature. The line is the best fit for rate $\propto(1+z)^{3.6}$, i.e. proportional to the SFR.

Canadian collaboration members acknowledge support from NSERC and CIAR; French collaboration members from CNRS/IN2P3, CNRS/INSU and CEA. SNLS relies on observations with MegaCam, a joint project of CFHT and CEA/DAPNIA, at the Canada-France-Hawaii Telescope (CFHT) which is operated by the National Research Council (NRC) of Canada, the Institut National des Science de l'Univers of the Centre National de la Recherche Scientifique (CNRS) of France, and the University of Hawaii. This work is based in part on data products produced at the Canadian Astronomy Data Centre as part of the Canada-France-Hawaii Telescope Legacy Survey, a collaborative project of the National Research Council of Canada and the French Centre national de la recherche scientifique.

References

Astier, P., Guy, J., Regnault, N., et al. 2006, A&A, 447, 31
Bazin, G. 2008, Ph.D. Thesis
Bazin, G., et al. 2009, in prep.
Bertin, E., & Arnouts, S. 1996, A&AS, 117, 39
Botticella, M. T., Riello, M., Cappellaro, E., et al. 2008, A&A, 479, 49
Cappellaro, E., Evans, R., & Turatto, M. 1999, A&A, 351, 459
Cappellaro, E., Riello, M., Altavilla, G., et al. 2005, A&A, 430, 83
Dahlen, T., Strolger, L.-G., Riess, A. G., et al. 2004, ApJ, 613, 189
Guy, J., Astier, P., Baumont, S., et al. 2007, A&A, 466, 11
Hatano, K., Branch, D., & Deaton, J. 1998, ApJ, 502, 177
Hopkins, A. M., & Beacom, J. F. 2006, ApJ, 651, 142
Ilbert, O., Arnouts, S., McCracken, H. J., et al. 2006, A&A, 457, 841I
Li, W., Filippenko, A., Treffers, V., Richard, R., et al. 2001, ApJ, 546, 734
Neill, J. D., Sullivan, M., Balam, D., et al. 2006, AJ, 132, 1126
Fukugita, M., Ichikawa, T., Gunn J., et al. 1996, AJ, 111, 1748
Pritchet, C., Howell, A., & Sullivan, M. 2008, ApJ, 683L, 25
Richardson, D., Branch, D., Casebeer, D., et al. 2002, AJ, 123, 745
Sullivan, M., Howell, D. A., Perrett, K., et al. 2006, AJ, 131, 960

[2] http://nedwww.ipac.caltech.edu/index.html